Outdoor performance evaluation of a holographic solar concentrator optimized for building integration

Julia Marín-Sáez,[1,2] Daniel Chemisana,[1,*] Jesús Atencia,[2] María-Victoria Collados[2].

[1]*Applied Physics Section of the Environmental Science Department, Polytechnic School, University of Lleida, Jaume II 69, 25001 Lleida, Spain*
[2]*Applied Physics Department, Aragon Institute of Engineering Research (I3A), Faculty of Science,University of Zaragoza, Pedro Cerbuna 12, 50009 Zaragoza, Spain*
* daniel.chemisana@macs.udl.cat

Abstract:

A holographic solar concentrating system with a Silicon photovoltaic (PV) cell is designed, constructed and characterized. The design is based on a previous system and is further optimized. The cylindrical holographic lenses forming the concentrating system are modeled with a ray-tracing algorithm based on Coupled Wave Theory and are recorded on Bayfol® HX photopolymer. Measurements are carried out outdoors with solar illumination and provide a current density of 146 mA/cm^2 with a current concentration factor of 3.48, validating the theoretical simulations results (172 mA/cm^2 and 3.81, respectively). The effect of the temperature on the performance of the Holographic Optical Elements (HOEs) is studied and taking it into account by assuming a 1.3º tilt of the fringes of the hologram caused by thermal expansion (which is reversible if the HOEs are encapsulated and sealed) provides simulation results closer to the experimental ones (a current density value of 155 mA/cm^2 and current concentration of 3.43). The ageing of HOEs recorded in Bayfol® HX photopolymer due to the outdoor environmental conditions is also analyzed, revealing the need of encapsulation and sealing.

Keywords: Building Integrated Photovoltaics, Solar Concentration, Holographic Concentrators, Holographic Optical Elements.

Glossary

HOE	Holographic Optical Element
PV	Photovoltaic
CPV	Concentrating Photovoltaic
θ	Angle that the projection of the incident sun rays on the YZ plane forms with *z*-axis
ϕ	Angle that the projection of the incident sun rays on the XZ plane forms with *z*-axis
c'_{Lz}	Directional cosine in *z*-direction of the L -diffraction order
A_L	Amplitude of the L -diffraction order wave
ϑ_L	Dephasing parameter of the L -order
n_1	Index modulation
λ	Reconstruction wavelength
$\vec{p}_L$	Polarization vector of the L -order
$CC_{current,\lambda}$	Concentration of generated electrical current for each wavelength

$I_{SC,\,HOEs,\,\lambda}$	Electrical current generated with the concentrating system for each wavelength
$I_{SC,\,no\ HOEs,\,\lambda}$	Electrical current generated without the concentrating system for each wavelength
$CC_{current}$	Concentration of generated electrical current
$I_{SC,\,HOEs}$	Electrical current generated with the concentrating system
$I_{SC,\,no\ HOEs}$	Electrical current generated without the concentrating system
J_{SC}	Electrical current density generated at short circuit

1. Introduction

The integration of solar photovoltaic systems in buildings represents a potential way of reducing their energy consumption. In addition, since the energy is generated on-site, costs and losses associated to transmission and distribution of electricity are minimized and thus the system efficiency is enhanced. On the other hand, by incorporating a concentrating element the size of photovoltaic (PV) cells is decreased and related environmental impact and economic issues are improved, leading to a more cost-effective and green technology [1]. Among solar concentrators for building-integrated photovoltaics, Holographic Optical Elements (HOEs) are positioned as advantageous option due to two main factors [2]. The first is related to the chromatic selectivity and dispersion that enable the coupling of the spectral response curve of the PV cell with the solar spectrum so that wavelengths outside the spectral response of the PV cell are not concentrated. This implies the avoidance of overheating without having to use cooling systems, which can be a drawback in building-integrated systems. The second is in regard with the diffraction efficiency due to the angular selectivity of the hologram, which makes it totally see-through and improves building integration features with respect to conventional refractive or reflective optical elements.

There are currently several publications where HOEs are proposed as solar concentrators for photovoltaics systems. In most studies they are only characterized in the laboratory with monochromatic light sources. Among the existing publications where the holographic concentrator is illuminated with white light and measurements with a PV cell are performed [3–6], no modeling of the irradiance that reaches the PV cell is carried out. This is an important aspect of the study of HOEs, since it allows the optimization of the system for each configuration and the understanding of its behavior. The experimental study of other authors shows current concentration factors (the ratio of the generated electrical current with and without the concentrating system) of 1.23 [3], 1.27 [6], 1.80 [4], and 1.93 [5].

A holographic concentrator was previously proposed by the authors, modeled with a ray-tracing algorithm and experimentally characterized locally in the laboratory by illuminating the HOEs with an 800 nm laser, thus validating the calculations [7–9]. In reference [7] a volume cylindrical holographic lens was considered in order to evaluate the suitability of a holographic solar concentrator for a building-integrated hybrid photovoltaic-thermal system. Year-round simulations were carried out for two different locations in the Northern hemisphere, with positive results. In [8,9] three different designs of the holographic lenses were studied, each one comprising a different range of spatial frequencies and index modulations. It was determined that using HOEs partly operating in the transition regime was very advantageous for solar applications. HOEs have been recorded in the photosensitive material Bayfol® HX photopolymer, manufactured by Covestro Deutschland AG [10]. It was determined that it can

reach the required range of index modulation values to operate adequately in the bandwidth where silicon PV cells are more efficient [11]. This material was chosen due to the advantages it offers, including the lack of requirement of a thermal or chemical post-processing (as opposed to the other commonly used recording material, dichromated gelatin), allowing a future mass production of HOEs [12].

Furthermore, the environmental conditions need to be considered when analyzing the performance of HOEs for solar applications, because they cannot be controlled as in other indoors applications. The performance of a HOE in the laboratory (e.g. with set room temperature and humidity) differs from its performance outdoors, with varying ambient conditions throughout the day and the year and depending on the location. This is because the photosensitive material where the HOE is recorded may also be sensitive to these factors [13–17]; in fact they may be used as sensors [13,14]. Some authors have investigated the response of HOEs recorded on Bayfol® HX photopolymer while being at cryogenic temperatures [18], but there is no research analyzing the behavior of the hologram at temperatures that could be achieved outdoors.

Another important aspect in the evaluation of HOEs for this application is the degradation that they may suffer due to the prolonged exposure to the aforementioned outdoor conditions. Some authors have studied this with different photopolymer recording materials, reporting changes [19] such as efficiency loss [5,6]. Regarding HOEs recorded in Bayfol® HX photopolymer, Zanutta et al. [18] noted slight changes after being exposed to cycles of one week of duration at 40ºC. However, Chrysler et al. [20] attached sealed HOEs recorded in Bayfol® HX 102 photopolymer to a Silicon PV panel placed outdoors and took measurements every four weeks, noticing substantial changes in the gratings and the material itself already after the first four weeks (but do not provide the temperatures that the HOEs are exposed to although they state that typical PV cell temperatures reach 80ºC in summer). Nevertheless, in most solar applications the HOEs are not placed directly attached to the PV cells but at a certain distance, and then the HOEs temperature will not increase that much. Therefore, further investigation about ageing should be carried out in general and specially for each considered configuration.

Based on the references presented above, it can be seen that albeit the big potential of holographic concentrators for building-integrated solar applications there are few rigorous studies dealing with the topic and more research is needed for better comprehension of their performance and reliability under real operating conditions. In order to fill this gap, the present study describes a holographic concentrator that doubles the concentration ratio of those found in the literature, leading to a higher cost-effectiveness. The system, which had been optimized considering both the solar spectrum and the spectral response of the PV cell, is fabricated and assessed outdoors determining optical and electrical performances under real conditions of operation, namely solar illumination and outdoor summer temperatures. The obtained results are compared with theoretical calculations, in order to validate the global performance that is modeled. In addition, temperature and ageing effects on the HOEs are also addressed to analyze their suitability for solar applications.

This article is structured as follows: the holographic concentrating system is described in section 2, comprising the optical design (subsection 2.1) and the fabrication of the HOEs (subsection 2.2) and the results are presented in section 3, which is divided in three parts. Subsection 3.1 covers the experimental study of the performance of the holographic concentrating system under sunlight illumination and its comparison with the theoretical simulations. An analysis of the

response of the HOEs under different temperatures of operation is included in subsection 3.2. An ageing study of the HOEs at summer outdoor conditions can be found in subsection 3.3. Finally, the conclusions are presented in section 4.

2. Description of the Holographic Concentrating System

A solar concentrating photovoltaic system formed by two identical HOEs and a conventional mono-crystalline Si PV cell, shown in figure 1(a), is studied in this work. The two HOEs are cylindrical lenses and are placed symmetrically at the same XY-plane so that sunlight incident on each one of them is diffracted towards the same PV cell. There is a separation between the two HOEs, where light is simply transmitted. Figure 1(c) shows the way the system would be integrated in the solar shading louvers in a South-oriented façade of a building in the Northern hemisphere (or a North-oriented façade in the Southern hemisphere). The blinds track the solar altitude movement, and that means that θ (the angle that the projection of the incident sun rays on the YZ plane forms with *z*-axis) is kept equal to zero at every moment and ϕ (the angle that the projection of the incident sun rays on the XZ plane forms with *z*-axis) is allowed to vary. The system is placed in such a way that the direction with tracking matches the direction of high angular selectivity of the HOEs and the direction without tracking matches the direction of low angular selectivity, as depicted in Figure 1(b). This configuration was already proposed in previous publications [7–9] by the authors, where the HOEs and the system's dimensions were at earlier design stages.

2.1. Optical design

The holographic cylindrical lenses are recorded by interfering a plane wave with a cylindrical wave, so when illuminating them with a plane wave a cylindrical wave is obtained at its output. This cylindrical wave will focalize at a different locus for each illumination wavelength. Since solar light can be assumed to have a plane wavefront, it is concentrated onto a linear spot.

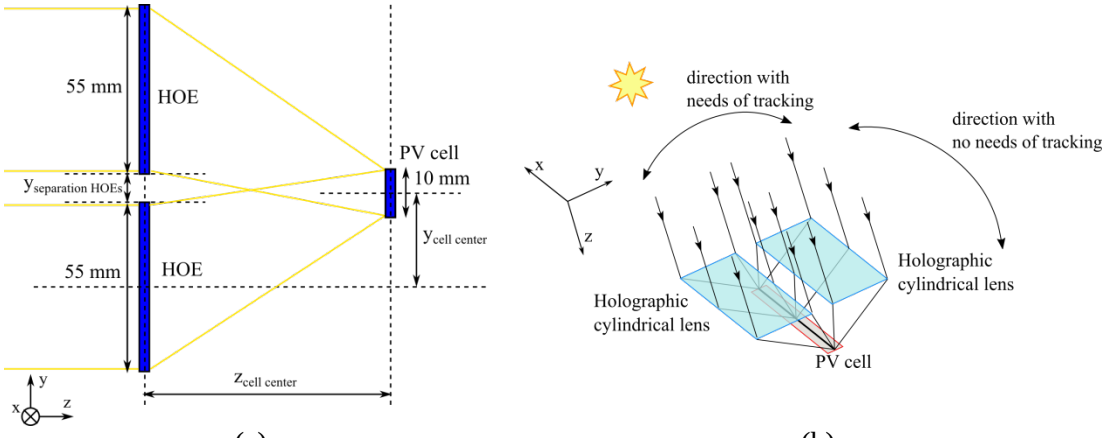

(a) (b)

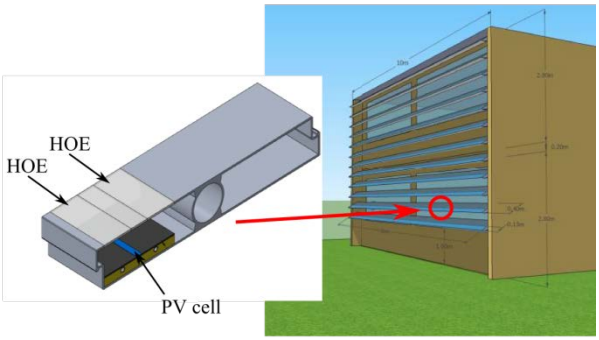

(c)

Figure 1. (a) Holographic concentrating system: two cylindrical holographic lenses redirect sunrays towards the PV cell; (b) Directions with and without need of tracking; (c) Integration of the system in the solar shading louvers of a building façade [7].

In the case of a volume hologram (a hologram operating in the volume regime), only two beams are found: the transmitted beam or 0^{th} order, and the diffracted beam, or 1^{st} order of diffraction. However, in the general case of holograms not operating in the volume regime, more diffraction orders emerge, and the incident energy is distributed among them. It was found in a previous study[8] that HOEs partly performing in the transition regime are more suitable for solar concentration than HOEs operating entirely in the volume regime. This is due to several factors, including the lower angular and chromatic selectivity and dispersion of HOEs in the transition regime. Based on the authors' previous findings, the present hologram is designed partly operating in the transition regime and is optimized under the solar spectrum illumination to maximize PV electrical output.

The design and associated model is performed with a ray-tracing algorithm with an energetic modeling based on Coupled Wave Theory [21] developed in MATLAB. Further description of the model can be found in [8,22,23]. The efficiency of each diffraction order L is given by the coupled differential equations

$$c'_{Lz}\frac{dA_L}{dz} + j\vartheta_L A_L + j\frac{\pi n_1}{\lambda}\left[A_{L+1}\left(\vec{p}_{L+1}\cdot\vec{p}_L\right) + A_{L-1}\left(\vec{p}_{L-1}\cdot\vec{p}_L\right)\right] = 0 \qquad (1)$$

where c'_{Lz} is the directional cosine in z-direction of the L-diffraction order, A_L is the amplitude of the L-diffraction order wave, ϑ_L is the dephasing parameter of the L-order (that quantifies the deviation of the reconstruction conditions from the optimal ones of the recorded grating), n_1 the index modulation, λ the reconstruction (or illumination) wavelength and $\vec{p}_L$ the polarization vector of the L-order.

The coupled differential equations (1) are numerically solved for each diffraction order L, reconstruction wavelength and angle of incidence at each point of the HOE ("local grating" approach). Since sunlight is depolarized the coupled differential equations are solved for two perpendicular polarizations (one perpendicular to the recording plane and one contained in it, whose behavior is independent of one another) and the resulting efficiency of each one is averaged to obtain the final efficiency.

The optical concentration yielded by HOEs is different for each wavelength, so the concentrated spectral irradiance curve has a different shape from that of the incident solar spectrum. Since each wavelength produces a different current intensity response at the PV cell a global ratio of

the optical concentration is not an appropriate value to describe the system's concentration. Thus, the concentration of generated electrical current for each wavelength is defined instead, given by

$$CC_{current,\,\lambda} = \frac{I_{SC,\,HOEs,\,\lambda}}{I_{SC,\,no\,HOEs,\,\lambda}} \tag{2}$$

It is the ratio of the electrical current generated with the concentrating system over the one without the concentrating system for each wavelength [8]. The overall concentration of electrical current is calculated by integrating the electrical current,

$$CC_{current} = \frac{I_{SC,\,HOEs}}{I_{SC,\,no\,HOEs}} = \frac{\int I_{SC,\,HOEs,\,\lambda}\,d\lambda}{\int I_{SC,\,no\,HOEs,\,\lambda}\,d\lambda} \tag{3}$$

Sunlight on the Earth's surface is composed by direct and diffuse radiation. The reliability of this ray-tracing modeling is limited by the percentage of direct radiation, which depends on the clearness of the atmosphere at each location.

The *y*-distance between the two HOEs and the (*y*,*z*) position of the PV cell were optimized so that the PV cell would generate maximal current density averaged over the range $-60° < \phi < 60°$. It was chosen to optimize those parameters over a range of incidence angles in order to consider the variation of the Sun position in the sky throughout the day. Otherwise, if the optimization was carried out with $\phi = 0°$, at solar midday, the performance at that moment would be the best, but the overall performance of the day would be worse. The angular range $-60° < \phi < 60°$ corresponds to a time period of roughly 4 hours during the summer solstice, 9 hours during the winter solstice (the whole day) and 6.5 hours during the spring and autumn equinoxes for a location with 42°N latitude. The dimensions of the system resulting from the optimization and marked in Figure 1(a) are presented in Table 1. The geometrical concentration is equal to 11.5x, since the *y*-dimension of each HOE is 5.5 times larger than the one of the cell, as shown in Figure 1(a), and the *y*-separation between the lenses is half of the *y*-dimension of the PV cell. The theoretical current concentration $CC_{current}$ obtained with perpendicular incidence is 3.8, considering the standard AM1.5D spectrum as the incident one on the system.

Table 1. Geometry of the concentrating system depicted in figure 1(a).

y-separation HOEs (mm)	$y_{\text{cell center}}$ (mm)	$z_{\text{cell center}}$ (mm)
5.0	30.0	60.6

Since tracking is only carried out in the solar altitude movement direction, at solar noon the illumination of the HOEs will be perpendicular, but not during the rest of the day. The direction with no tracking (azimuth direction) is matched with the direction of low angular selectivity, as mentioned in the introduction, but if the angle of incidence is rather far away from $\phi = 0°$ then several factors (such as the decrease in efficiency, the increase in dispersion, total internal reflection, etc) will cause a remarkable overall loss in the generated current. In order to quantify this, the ϕ-acceptance is defined as the angular ϕ range for which the generated current is above 90% of the maximal. Simulations were carried out with incident angles in the range $0° \leq \phi \leq 60°$, with a step size of 2°, and the resulting normalized current concentration values are

presented in Figure 2(a). The behavior with negative values of ϕ is the same as with positive values, therefore the horizontal axis shows absolute values of ϕ.

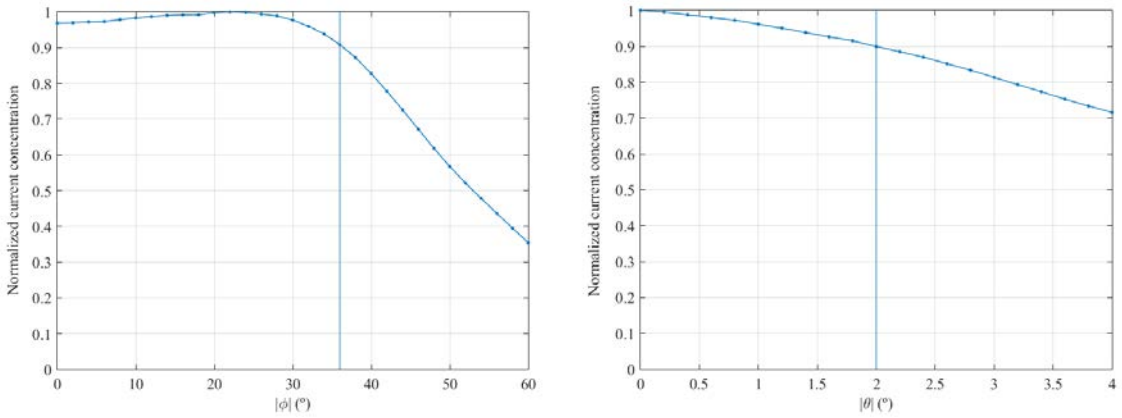

(a) (b)

Figure 2 (a) ϕ-acceptance, (b) θ-acceptance.

The optimal performance is not found with perpendicular incidence, but at ϕ=22º, with a current intensity approximately 3% higher, because the position of the PV cell and the distance between the lenses was optimized taking an angular range into account, as mentioned before. The ϕ-acceptance of this system is 72º (-36º< ϕ <36º), which corresponds to a time period of roughly 2 hours during the summer solstice, 5 hours during the winter solstice and 3.5 hours during the spring and autumn equinoxes for a location with 42°N latitude. The electrical current is higher with the concentrating system in place than without it for the whole considered angular range.

Even though tracking is carried out in the solar altitude direction, the tracking systems are not perfect and the tilt is corrected every certain amount of time. Simulations were also carried out in order to find out the θ-acceptance of the system when ϕ=0°, which gives an idea of how accurate the tracking must be. The results are presented in Figure 2(b), showing a θ-acceptance of 4º (-2º< θ <2º) while keeping ϕ=0°. This allows the use of less demanding, low-cost trackers, since their tracking errors are within that range [24]. Again, absolute values of θ are plotted because the system's behavior is symmetrical with θ (although not the behavior of a single HOE).

2.2. Fabrication of the holographic lenses

The recording parameters of the HOEs are presented in table 2 and marked in figure 3(a). They were all selected so that the HOE would provide maximal efficiency in the 1st diffracted order (shown in figure 3(b) with the paraxial approximation) when reconstructing with 800 nm rays at perpendicular incidence. The exposure dosage was such that provided index modulation at each point of the lens given by $n_1 = 2.469 \cdot 10^{-5} SF + 0.0126$, optimized with the experimental procedure explained in [8], where SF is the spatial frequency of each point expressed in lines/mm. Of course, if the illumination wavelength is different from 800 nm then the direction of the diffracted rays is different, as illustrated in figure 3(c), and their efficiency will be lower.

Table 2. Recording parameters of the cylindrical holographic lenses, marked in figure 3(a).

$\theta_{c,\,center}$ (º)	θ_p (º)	z_{focus} (mm)	$\lambda_{recording}$ (nm)	Exposure dosage (mJ/cm^2)
19.1	3.8	105	532	14

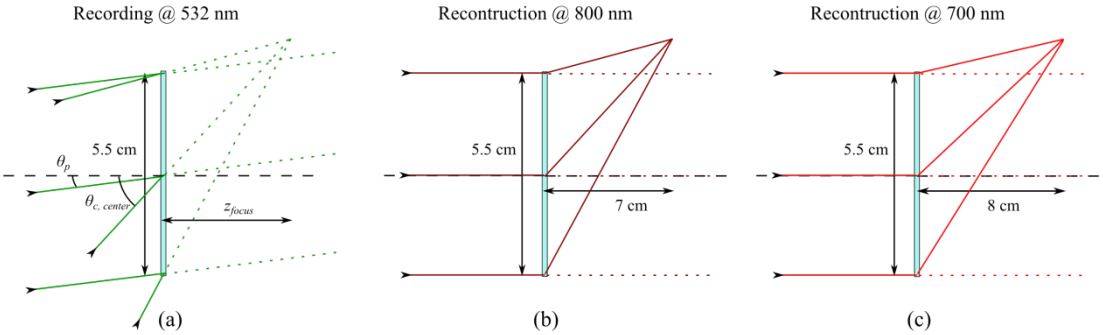

Figure 3. Recording scheme at 532 nm (a) and reconstruction with perpendicular incidence at 800 nm (b) and 700 nm (c) considering the paraxial approximation.

Holograms were recorded on Bayfol® HX 200, which is formed by a photopolymer layer and a cellulose triacetate substrate layer. Each Bayfol® HX 200 film sample was laminated on a glass slide by applying pressure with a soft roller, as indicated by the manufacturer [25] (with the photopolymer side of the sample in contact with the glass slide). A HOE was then recorded with the setup in figure 4 for the case of a cylindrical holographic lens. For the recording of holographic gratings that will be utilized in the temperature and the ageing studies (Sections 3.2 and 3.3), the cylindrical lens of the setup was removed. No post-processing was needed after the recording [10], only incoherent light photocuring, which was carried out as detailed in [11].

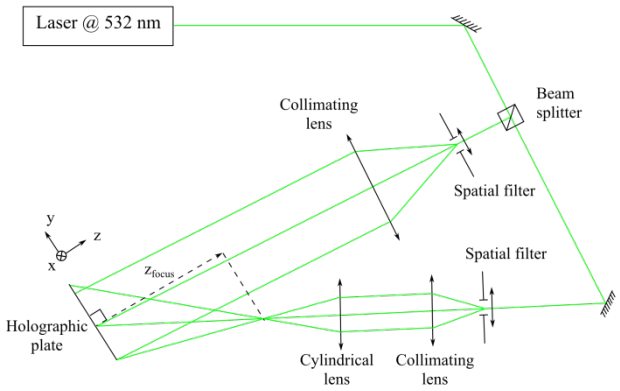

Figure 4: Recording setup of a cylindrical holographic lens [8].

3. Results and discussion

3.1. Sunlight illumination measurements

Experiments with the holographic concentrating system described in section 2 were carried out outdoors with solar illumination during the first week of August 2018 at the University of Lleida, Spain (41º37'N, 0º38'E).

A heliostat directed sun rays towards a testing unit. The holographic concentrating photovoltaic (CPV) system was placed inside in such a way that the incidence of the sun rays on the glass slides where the HOEs were laminated was perpendicular. A pyranometer (Kipp&Zonen CMP6) and a pyrheliometer (Kipp&Zonen CHP1) were fixed next to the CPV system and also

perpendicular to the incident sun rays to measure the global and direct irradiance, respectively. These data were sent to a Data Acquisition System DAQs (Campbell Sci. CR1000) and monitored throughout the whole experiment. The temperatures of the HOEs and the PV cell were measured by attaching T-type thermocouples to one of the corners of the HOE (shielded to prevent sunlight effects) and to the rear of the PV cell.

This experiment is divided in two parts: characterization of spectral irradiance and characterization of electrical performance. During the first part of the experiment the detector of a spectrometer (Ocean Optics USB4000, with a diameter of 3.9 mm and a sensitivity range from 350 to 1030 nm) was used to measure the incident solar spectrum. It is shown in figure 5 with a dot-dashed red line along with the standard spectrum normalized to the direct irradiance measured by the pyrheliometer during the experiment with a continuous blue line for comparison. Both curves include Fresnel reflection losses on the surface of the PV cell. It is noticed that the measured spectrum matches well the AM1.5D one.

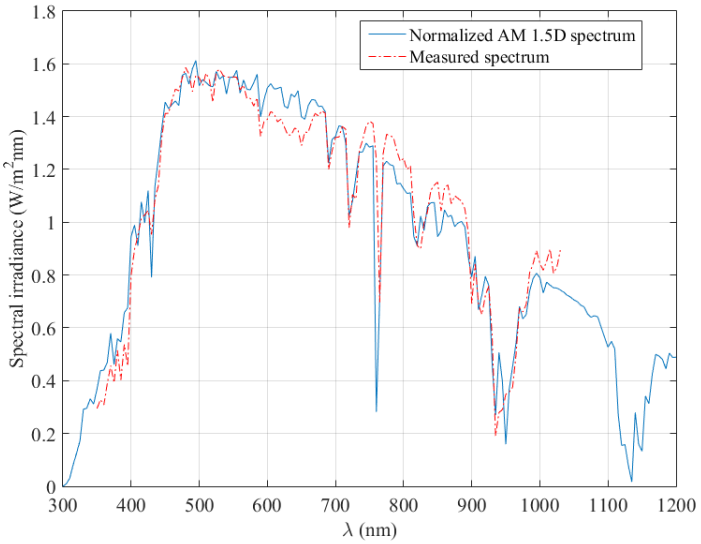

Figure 5: Standard solar spectrum AM1.5D normalized to the measured direct irradiance (continuous blue line), and measured spectrum (dot-dashed red line).

The detector was then placed at the center of the position where the PV cell would be located, characterizing the spectral irradiance produced by the holographic concentrator. The spectral irradiance measured at that location is plotted in figure 6(a) with markers. The noise at the limits of the measured data is due to the detector's sensitivity range. The spectral irradiance on the surface of the detector was modeled (using the measured solar spectrum as incident spectrum) and calculated as the addition of the contribution of the lower lens, the upper lens and the space between lenses and the resulting curve is plotted in figure 6(a) with a continuous line. Good agreement between the theoretical and experimental data is observed, with some differences between them, especially for wavelengths shorter than 700 nm. The peak centered on roughly 900 nm corresponds to rays of the 1st order of diffraction of both lenses, whereas the peak on approximately 450 nm, to the 2nd order of diffraction of both lenses as well.

This process was repeated for another position of the detector towards the edge of the PV cell's position and the results are plotted in figure 6(b), showing reasonably good agreement between the experimental and simulation data. The peaks at 800 nm and 400 nm correspond to the 1st and

2nd order of diffraction respectively of the lower lens. The peaks corresponding to the upper lens are not coincident in this case because the detector is not placed at a position symmetric with the HOEs.

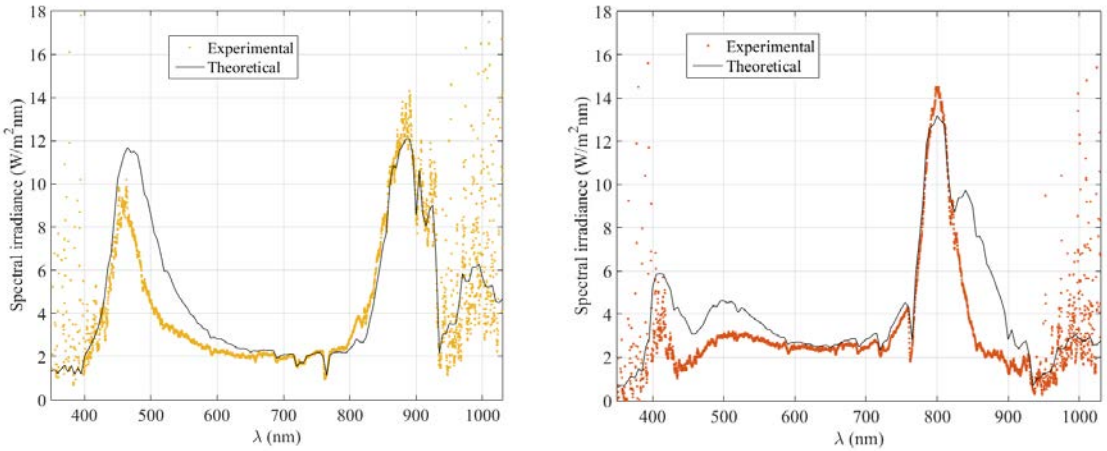

(a) (b)

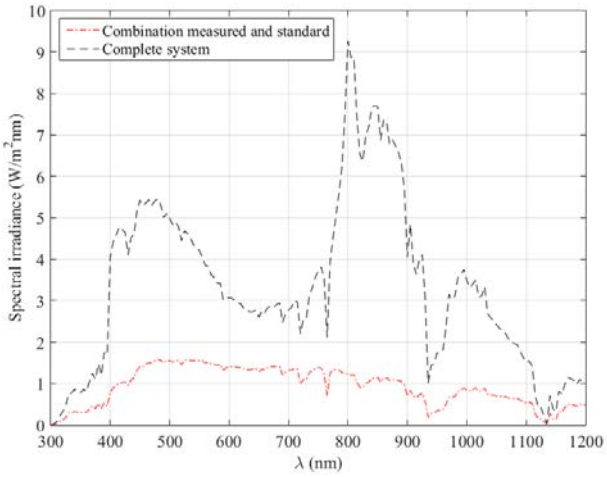

(c)

Figure 6: Experimental (markers) and simulated (continuous line) spectral irradiance received by the detector placed at the center of the position of the PV cell (a) and at a position towards its edge (b). Modelled spectrum received by the PV cell due to the concentrating system (dashed black line) and measured solar spectrum incident on the system, completed with standard spectrum (dot-dashed red line) (c).

These results confirm the validity of the modeling algorithm used in this study. The small differences observed between theoretical and experimental results are later addressed. The modelled spectral irradiance that would reach the whole surface of the PV cell is obtained by integration and it is illustrated in Figure 6 (c). In order to have data from 300 to 350 nm and from 1030 to 1200 nm, out of the spectrometer range, and extend the measured spectral range to the whole sensitivity range of the PV cell, the measured incident solar spectrum was completed with the standard AM1.5D spectrum. It can be seen that the obtained result is a partial combination of the two local spectra charted in Figs. 6 (a) and (b).

During the second part of the experiment a 1 cm x 1 cm PV cell was placed at the optimized position determined in section 2. The experiment was carried out with a PV cell of that size

instead of 1 cm x 5 cm (which are the design dimensions when using HOEs of 5 cm x 5 cm) for simplicity and avoidance of possible vignetting effects. This does not alter any result because there is no concentration in *x*-direction, so only a 1 cm-wide section in *x*-direction of the HOEs is considered instead of the whole surface. A picture of the system is shown in figure 7(a).

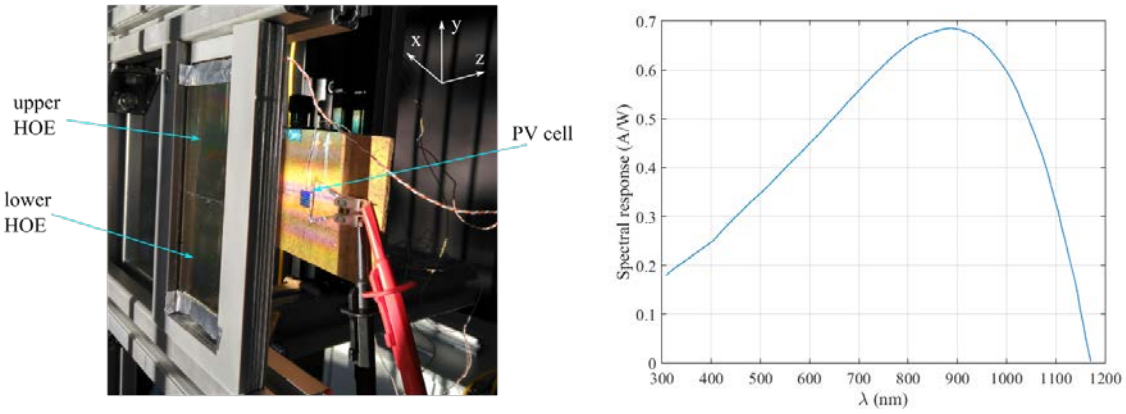

(a) (b)

Figure 7: (a) Picture of part of the setup for the measurement of the IV curves of the PV cell: two cylindrical holographic lenses on the left and a PV cell at the center of the picture; (b) Spectral response curve of the PV cell.

The PV cell was connected to a source meter (Keithley 2460) and a characteristic intensity-voltage (IV) curve without the HOEs was measured first, to determine the electrical performance of the PV cell under normal solar illumination. It is plotted in figure 8 with blue, non-filled markers. It should be noted that these values correspond to the contribution of both the direct and the diffuse irradiance that reaches the PV cell. Then the holographic concentrator was placed and the IV curve was measured again, presented in figure 8 as well, with red filled markers. The current generated at short-circuit conditions corresponding to the direct irradiance extracted from figure 8 is presented in table 3 for both cases.

The current density generated by the PV cell at short circuit conditions with and without the concentrating system was calculated from the spectral irradiance that the PV cell would receive (previously determined and shown in figure 6(c)) and the spectral response of the cell (figure 7(b)), obtaining the theoretical values in table 3. The calculated current density without the concentrating system (45 mA/cm^2) is lower than the measured one plotted in figure 8 (around 56 mA/cm^2) because in the simulations only the direct radiation is taken into account but in reality both direct and diffuse radiation contribute to the generation of electrical current. As mentioned in section 2, the ray-tracing algorithm developed to model HOEs is limited by the consideration of solely direct radiation.

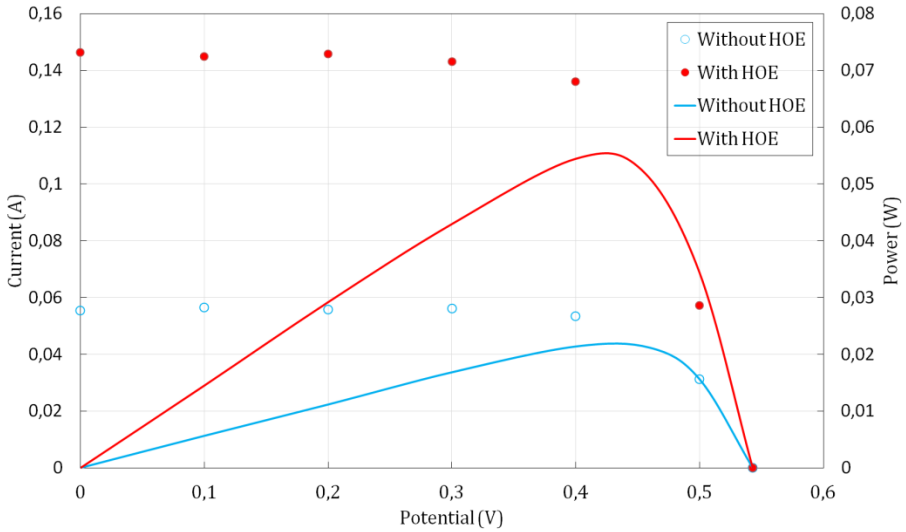

Figure 8: Experimental IV curves obtained with (red filled markers) and without the HOEs (blue non-filled markers) due to the direct and global irradiance, respectively. Calculated power-potential curves of the system with HOEs (continuous red line) and without (continuous blue line).

Table 3: Experimental and theoretical current density generated on the PV cell due to the direct irradiance.

	No concentrating elements	Holographic concentrating system	Current concentration
Experimental J_{sc} (mA/cm^2)	42	146	3.48
Theoretical J_{sc} (mA/cm^2)	45	172	3.81

The measured current density when the concentrating system is placed is 15% lower than the theoretical one. This difference can be attributed to some factors that may cause the performance of HOEs to worsen. One of them is the temperature of the HOEs during the experiment, which ranged between 37 and 49ºC, whereas the HOEs were designed to operate at room temperature. A study of the temperature dependence of HOEs recorded in Bayfol® HX 200 photopolymer is carried out in subsection 4.3 along with an estimation of the change in current.

In regard to the maximum power produced, the bare PV cell delivers 21.4 mW whereas the CPV system increases this value up to 55.2 mW. It can be appreciated that the power increases in a ratio of 2.58. This lower ratio related to the one obtained through the short-circuit current quotient is attributed to the fill factor. Fill factor of both curves takes almost the same value rounding 76% (74.5% -with concentrator - and 77.0% -without concentrator). On the other hand, as indicated previously, since the holographic concentrator only focus towards the PVs a certain bandwidth around the PV cell maximal spectral response, the temperature reached in both configurations does not differ substantially (4.94 ºC). Taking into account the temperature coefficient of crystalline silicon solar cells of around -0.3 %/ºC, the temperature difference registered would mean an open-circuit potential reduction of ~8 mV with respect to a value of 540 mW (see Fig. 8). Conversely, a logarithmic increase in the open-circuit potential is experienced due to the concentrated flux that counteracts the small potential decrease pointed

out. As a result, almost no variation over the open-circuit potential was measured, 544 mV for the bare PV and in 543 mV for the CPV.

Taking these considerations into account the concordance between theoretical and experimental results is reasonably good. Besides, in the next subsection a further analysis regarding temperature effects that could cause the small differences pointed out above is carried out. It is worth mentioning that the concentration ratio obtained for the present device is higher than that of other holographic concentrating systems found in the literature [3–6].

3.2. Study of the temperature dependence

An experiment was carried out to investigate the variation of the response of HOEs recorded in Bayfol® HX 200 at different temperatures. A slanted holographic grating was used for a more precise analysis. The advantage of using a slanted grating as opposed to an unslanted grating is that changes in the thickness of the photopolymer layer are more easily noticeable.

The HOE was illuminated perpendicularly with an unpolarized white light beam (Mikropack Halogen light source HL-2000) and the transmitted spectrum was measured with a spectrometer (Ocean Optics USB4000). The HOE was placed inside a plastic box with an open base and two holes to allow the incident beam to go through, as shown in the setup scheme in figure 9(a). An adjustable heater was placed underneath to increase the temperature in a controlled manner, with a honeycomb channels structure on top in order to avoid convection cycles. A T-type thermocouple was attached to the HOE to monitor the temperature with a Data Acquisition System DAQs (Campbell Sci. CR1000). The transmitted spectrum was measured at room temperature and while increasing it in steps of roughly 4°C up to 60°C, which is the highest temperature before Bayfol® HX 200's substrate may suffer deformation according to the manufacturer [25]. Then the temperature was decreased and measurements at the same temperature steps were taken.

When increasing the temperature, a shift of the transmitted spectrum towards shorter wavelengths, an increase of the minimum transmittance, i.e., a decrease of the efficiency of the 1st diffracted order, and a narrowing of the spectrum are noticed. The spectra measured when increasing the temperature did not match the ones measured when decreasing it (neither position nor transmittance of the minimum). The deviation from the initial central wavelength of the diffracted spectrum at different temperatures is presented in figure 9(b), showing maximal wavelength variations of 12 nm between the increase and decrease of the temperature. This is believed to be caused by a non-reversible thermal deformation of the photopolymer and/or the substrate layer. The experiment was repeated on different days and the same tendency was found.

In order to avoid this, another slanted holographic grating was encapsulated after the recording and bleaching. An optical adhesive, Norland NOA61 was extended on the substrate side of Bayfol® HX and another glass slide was placed on top. Some optical adhesive was also poured on all four glass borders in order to completely encapsulate the sample.

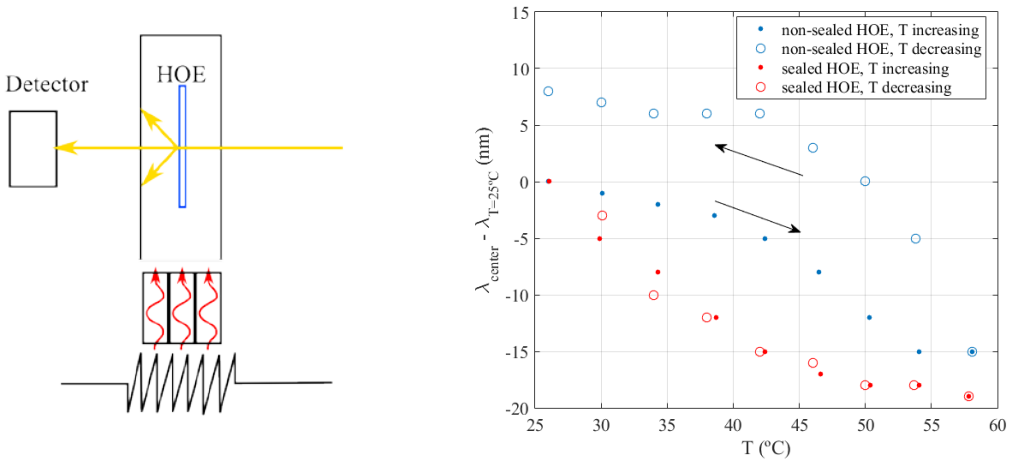

(a) (b)

Figure 9. (a) Experimental setup scheme for the temperature study; (b) Deviation from the central wavelength at room-temperature when varying the temperature for non-sealed (blue markers) and sealed (red markers) HOEs when increasing (filled markers) and decreasing (non-filled markers) the temperature.

The experiment was then carried out with the sealed holographic grating. Similar variations were observed when increasing the temperature, but in this case the measured spectra while decreasing it did match the spectra measured when increasing it, as shown in figure 9(b) as well, with maximal wavelength deviations of 2 nm between the increase and decrease of temperature. Therefore, sealing the HOE prevented irreversible thermal expansion from occurring at this stage. The measured spectra while increasing the temperature are presented in figure 10.

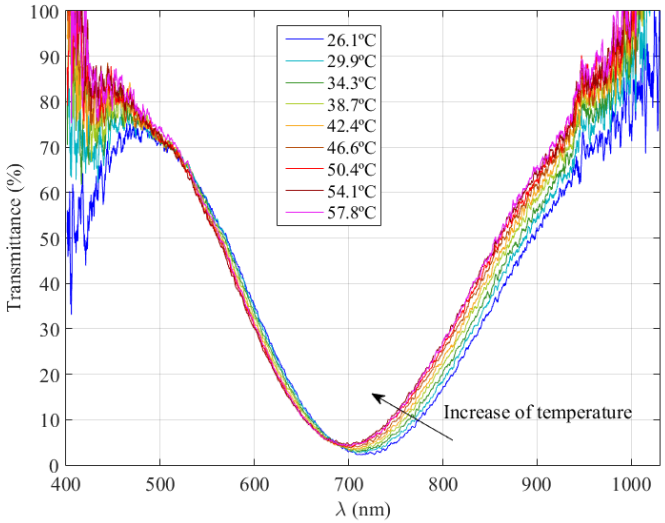

Figure 10: Transmission spectra when increasing the temperature.

The shift of the transmitted spectrum towards shorter wavelengths and simultaneous decrease in efficiency are consistent with two effects: thermal expansion of the photopolymer layer, which causes the slant of the grating to change increasing the spatial frequency, and a decrease of the index modulation. This was already suggested by other authors working with other photopolymer compositions (first effect by [14,15,17] and second effect by [14]).

Since the change in temperature causes a change in the response of the HOEs this should be included in the theoretical model as well in order to improve it so that the HOEs are optimized for the average operation temperature throughout the year, instead of at room temperature. However, the system is rather complex (a glass slide, photopolymer layer, substrate layer, optical adhesive and another glass slide, as well as optical adhesive on all four edges), and further research would be needed to obtain a mathematical model of all the thermal expansions and the resulting tensions among the different components and their effect on the refractive index, thickness and slant of the fringes.

A preliminary estimation resulting from this study was to consider a change of the slant of the fringes, compatible with an expansion of the photopolymer layer at high temperatures. The theoretical simulations of subsection 3.1 were repeated assuming a 1.3º tilt of the slant and the spectral irradiance that would be received by the detector is then plotted in figure 11(a) and (b). The agreement between experimental and theoretical data is better in this case than in figure 6.

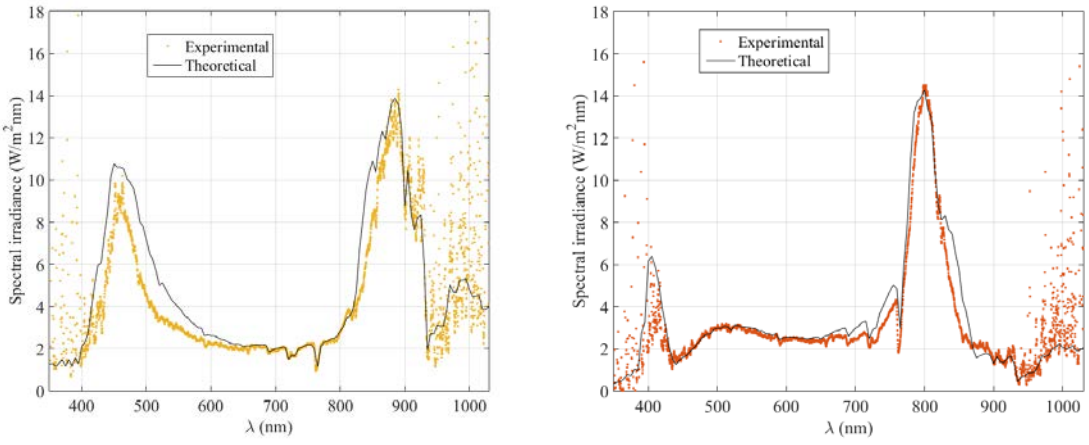

(a) (b)

Figure 11: Experimental (markers) and simulated (continuous line) spectral irradiance received by the detector placed at the center of the position of the PV cell (a) and at a position towards its edge (b).

The electrical current density obtained with this assumption is 155 mA/cm^2 and the current concentration, 3.43. These values are closer to the experimentally obtained ones in the previous subsection.

3.3. Study of ageing

A study of the possible degradation due to environmental conditions of HOEs recorded in Bayfol® HX photopolymer was carried out outdoors. Six cylindrical holographic lenses (named samples L1-L6), two samples of bleached unrecorded Bayfol® HX 200 (named samples B1 and B2), and one sample of the substrate of Bayfol® HX 200 (named sample S1 and obtained by mechanically removing the photopolymer layer) were used. Some of them were encapsulated and others simply laminated on glass, as specified in table 4.

Lenses L5 and L6 were kept in the laboratory as control samples. The rest of samples were placed on the South-oriented façade of a testing unit outdoors at the University of Lleida's facilities, Spain (41º37'N, 0º38'E), during summer 2018. Lenses L1 and L2 were simply placed

on a metallic structure, indicated in table 4 as “Testing unit outdoors”. Samples L3, L4, B1, B2 and S1 were integrated as a box lid, in order to imitate the conditions of the solar shading louver where the concentrating system would be placed [7], which imply higher temperatures.

Table 4: Characteristics of holographic lenses and samples of bleached unrecorded Bayfol® HX 200 and substrate used during the degradation experiment.

Placement	Sample	Preparation	Outcome
Testing unit outdoors	L1	Laminated on glass	Deteriorated and detached
	L2	Encapsulated	No changes*
Testing unit outdoors, in box	L3	Laminated on glass	Deteriorated and detached
	L4	Encapsulated	No changes*
	B1	Laminated on glass	Detached
	B2	Encapsulated	No changes
	S1	Encapsulated	No changes
Laboratory	L5	Laminated on glass	No changes
	L6	Encapsulated	No changes*

* Indicates that a small increase of index modulation was observed after the sealing and encapsulation with the optical adhesive, but it stabilized after a few days.

Three T-type thermocouples were connected to a Data Acquisition Systems DAQs (Campbell Sci. CR1000) to monitor the temperature of the HOEs and samples placed inside the box, outside the box, and the ambient temperature. A pyranometer (Kipp&Zonen CMP6) was also placed on the façade to monitor the global irradiance. Temperature and irradiance data were stored every minute.

Figure 12 shows the recorded parameters on four summer days: two sunny days during a heat wave (figure 12(a)) and two cloudy days (figure 12(b)), to show different conditions. HOEs placed inside the box reached temperatures higher than 45ºC every day and higher than 50ºC during the hottest weeks of the summer. The maximal temperatures reached by the HOEs outside the box were approximately 5ºC lower, but remarkably higher than the air temperature during the central hours of the day. Since the whole setup was fixed at the South-oriented façade and tracking of the sun’s movement was not carried out, the global irradiance recorded by the pyranometer was lower on days closer to the summer solstice than at the end of the summer. The “side lobes” of the global irradiance curve shown in figure 12(a) are due to reflections on the opposite building’s windows, which reached the pyranometer at the start and end of the day around the summer solstice because of the large azimuth angles.

Every few days the samples were removed and characterized in the laboratory and then placed again on the testing unit. They were illuminated with an unpolarized white light source (Ocean Optics LS-1) and their spectral transmittance was measured with a spectrometer (Ocean Optics USB2000). They were also illuminated with an 800 nm laser (ThorLabs Laser Diode CPS808A, emitting 4.4 mW) while scanning the incidence angle and the transmitted beam was measured (with Newport Power Meter Model 1815-C with detector Model 818-SL, with an uncertainty of 5 μW). In the case of characterizing HOEs the first measurement provided their chromatic selectivity and the second one the angular selectivity. These measurements were carried out at three different points of the HOEs in order to study the behavior of different spatial frequencies and index modulations.

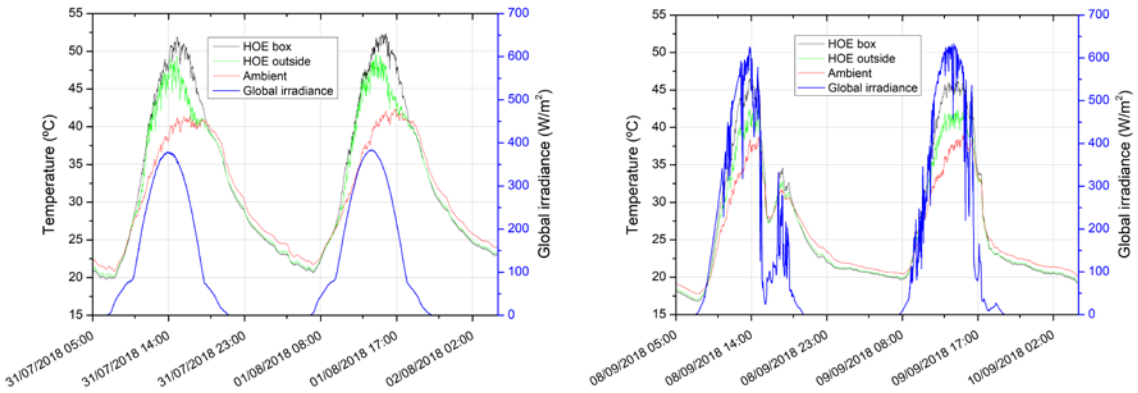

(a) (b)

Figure 12. Sample of the data recorded by the datalogger on four different days of the summer (two sunny days during a heat wave (a) and two cloudy days (b)): the temperature of HOEs inside the box (black line), outside the box (green line) and ambient temperature (red line), left *y*-axis, and the global irradiance measured in South-direction (blue line), right *y*-axis.

The following conclusions are extracted from the results of the measurements and summarized in table 4:

- Non-encapsulated lenses and samples detach from the glass where they are laminated and suffer deterioration due to the outdoor environmental conditions. Some of the angular selectivity measurements of L1 that illustrate the progression of the observed changes are represented in figure 13 (a). Two distinct stages are observed (which are not correlated with the first appearance of the detachment of the film from the glass slide). During the first phase (first 13 days of outdoor exposure) the position of the peaks does not change, and the efficiency of the 0 order decreases, while the efficiency of the 1st order increases. This corresponds to an increase in index modulation of approximately 11% from $n_1 = 0.0190$ to $n_1 = 0.0210$, while the grating vector $\vec{K}$ remains constant. Afterwards, a substantial shift in the position of the peaks occurs, meaning that the grating vector $\vec{K}$ has changed. These two behaviors were observed in the three points of the lens that were studied. They were also confirmed with the measurement of the chromatic selectivity. The first stage of this behavior is in agreement with the results of the temperature response of the non-sealed HOEs presented in section 3.3: after the heating and cooling cycle an increase of the index modulation of the grating is observed.
- Encapsulating Bayfol® HX photopolymer samples prevents them from detaching from the glass slide and preserves the material at least during the studied time period. Angular and chromatic selectivity measurements of the encapsulated HOEs L2, L4 and L6 only showed a slight difference between the first measurement (taken right after sealing) and the rest of the measurements. This corresponds to an increase in index modulation of approximately 2% and is associated with the optical adhesive, since no changes were observed in L5. Again, this behavior was confirmed in three different points of the sealed HOEs. Some representative angular selectivity curves of L4 are presented in figure 13 (b). Since the maximal efficiency of this HOE at 800 nm is approximately 100% this change is not perceptible at the peak itself but the change at the side lobes' efficiency is more noticeable. This corresponds to a change in index modulation from approximately $n_1 = 0.0231$ to $n_1 = 0.0236$. During the rest of the

experiment (37 days of exposure to outdoor ambient conditions) no further changes are observed. This is again in agreement with the results of the temperature response of the sealed HOEs presented in section 4.3: no changes are observed after the heating and cooling cycle.

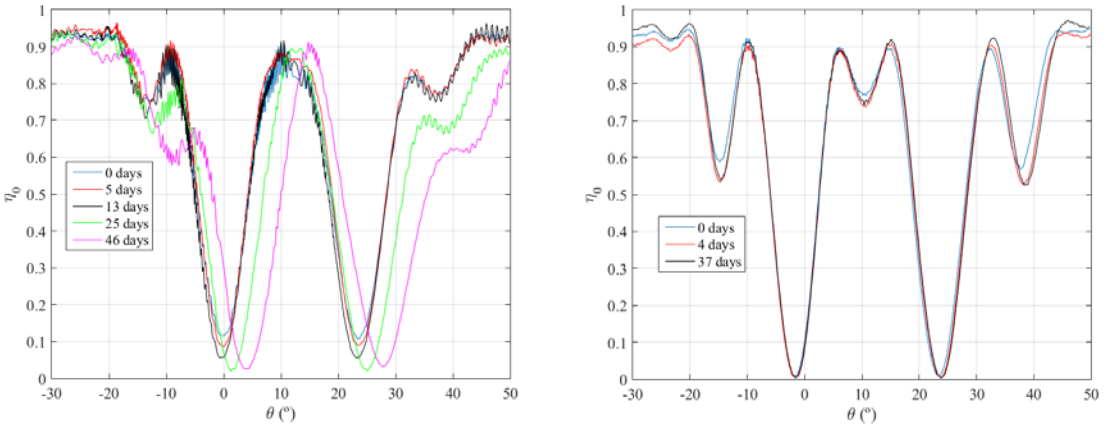

(a) (b)

Figure 13. Angular selectivity curves of a point of L1 (a) and a point of L4 (b) after several days of outdoor exposure.

It is concluded that although non-sealed HOEs recorded in Bayfol® HX 200 photopolymer are not suitable for outdoor applications, sealed HOEs have remained stable during the course of the study (except from the slight initial variation of index modulation) and seem to be appropriate for solar concentration applications. Although the results have been positive during the summer, when outdoor conditions are more extreme in this location, it is still necessary to continue this study for a longer period of time to verify the suitability of this material.

This does not contradict the results presented by Chrysler et al. [20], who also tested encapsulated gratings and samples of Bayfol® HX. They reported substantial changes both in the gratings (detected by measuring angular and chromatic selectivity) and in the material itself (by measuring the spectral transmittance of unrecorded samples) already after 4 weeks of outdoor exposure. Two factors are believed to cause this difference between the two studies. First, the recording material used by Chrysler et al was Bayfol® HX 102, which was substituted by Covestro Deutschland AG by Bayfol® HX 200 (the one used in the present study), so they are not exactly the same material and may have different properties. The substrate layer is indeed different: the substrate in Bayfol® HX 102 is made of polycarbonate [26], whereas the substrate in Bayfol® HX 200 is made of triacetate cellulose [25]. Second, Chrysler et al directly attached the HOEs to the PV cells, which may reach high temperatures (up to 80ºC [20]), while the manufacturer states that temperatures higher than 60ºC can lead to deformation of the substrate [26]. In the configuration considered in this study the HOEs are separated a certain distance from the PV cell, thus the temperature that they reach in our case would not be so heavily intensified by the temperature of the PV cell. The samples placed in the testing unit as a lid of a box (see table 4) imitate the conditions that the HOEs would experience when integrated as part of a double pane solar louver shading system, with higher temperatures than the ones of the samples outside the box (but still below 55ºC on the hottest days).

4. Conclusions

A holographic concentrating system comprising two cylindrical holographic lenses and a mono-crystalline Si PV cell was designed and optimized for building façade-integration on the blinds of a solar shading louver, which track the solar altitude movement. No tracking is needed in the azimuth direction, since the acceptance in that direction is 72º. The system was theoretically modeled with a ray-tracing algorithm based on Coupled Wave Theory, providing a current density value of 172 mA/cm^2 and current concentration ratio of 3.81 at perpendicular incidence. The HOEs, partially operating in the transition regime, were recorded on Bayfol® HX photopolymer and the system was assembled. Outdoor measurements of the diffracted spectrum with solar illumination yielded a current density value of 146 mA/cm^2 and a current concentration ratio of 3.48, somewhat lower than the simulated results but validating the theoretical model. The maximum power produced is increased in a ratio of 2.58, with a fill factor of 76% for both cases.

The difference between the theoretical and experimental current values is believed to be caused by a change in the holograms' internal structure due to the outdoor temperature, higher than room temperature, at which the HOEs had been designed and characterized. The temperature effect on HOEs recorded in Bayfol® HX photopolymer was studied, showing indeed variations when increasing the temperature, which are reversible if the HOE is encapsulated. Assuming a 1.3º tilt of the fringes in the holograms due to the outdoor temperature, better fits of the diffracted spectral curves and a theoretical current density of 155 mA/cm^2 and current concentration ratio of 3.43 were obtained, closer to the experimental ones.

A preliminary study of another important aspect for solar concentration, ageing of HOEs recorded in Bayfol® HX photopolymer, was carried out, showing that the recording material is suitable for solar concentration applications as long as the samples are sealed and encapsulated.

Future work is needed in order to analyze more thoroughly these two features: a model of the temperature response (which could allow the optimization of HOEs for higher temperatures) and an ageing study over a longer period of time.

Acknowledgements

The authors would like to thank Dr. Enrico Orselli (Covestro Deutschland AG) for supplying the recording photopolymer material. This research has been supported by the Spanish Ministerio de Economía y Competitividad (grants ENE2016-81040-R and FIS2015-71933-REDT), the Diputación General de Aragón-Fondo Social Europeo (TOL research group, E44_17R), the Universidad de Zaragoza (UZ2018-CIE-07) and the Generalitat de Catalunya (grants 2017 SGR 1276 and 2017FI_B2_00127).

References:

[1] Lamnatou C, Chemisana D. Concentrating solar systems: Life Cycle Assessment (LCA) and environmental issues. Renew Sustain Energy Rev 2017;78:916–32. doi:10.1016/j.rser.2017.04.065.

[2] Collados MV, Chemisana D, Atencia J. Holographic solar energy systems: The role of

optical elements. Renew Sustain Energy Rev 2016;59:130–40. doi:10.1016/j.rser.2015.12.260.

[3] Chemisana D, Collados MV, Quintanilla M, Atencia J. Holographic lenses for building integrated concentrating photovoltaics. Appl Energy 2013;110:227–35. doi:10.1016/j.apenergy.2013.04.049.

[4] Akbari H, Naydenova I, Ahmed H, McCormack S, Martin S. Development and testing of low spatial frequency holographic concentrator elements for collection of solar energy. Sol Energy 2017;155:103–9. doi:10.1016/j.solener.2017.04.067.

[5] Sreebha AB, Suresh S, Sreekala CO, Mahadevan Pillai VP. Volume holographic gratings in acrylamide-based photopolymer to provide selective light as an added input for improving the performance of dye-sensitized solar cells. Curr Sci 2018;114:2267–72. doi:10.18520/cs/v114/i11/2267-2272.

[6] Aswathy G, Rajesh CS, Sreejith MS, Vijayakumar KP, Sudha Kartha C. Designing photovoltaic concentrators using holographic lens recorded in nickel ion doped photopolymer material. Sol Energy 2018;163:70–7. doi:10.1016/j.solener.2018.01.017.

[7] Marín-Sáez J, Chemisana D, Moreno Á, Riverola A, Atencia J, Collados M-V. Energy Simulation of a Holographic PVT Concentrating System for Building Integration Applications. Energies 2016;9:577. doi:10.3390/en9080577.

[8] Marín-Sáez J, Atencia J, Chemisana D, Collados M-V. Full modeling and experimental validation of cylindrical holographic lenses recorded in Bayfol HX photopolymer and partly operating in the transition regime for solar concentration. Opt Express 2018;26:A398. doi:10.1364/OE.26.00A398.

[9] Marín-Sáez J, Collados MV, Chemisana D, Atencia J. Energy analysis of holographic lenses for solar concentration. In: Hrabovský M, Sheridan JT, Fimia A, editors. Proc. SPIE, 2017, p. 1023317. doi:10.1117/12.2265816.

[10] Jurbergs D, Bruder F-K, Deuber F, Facke T, Hagen R, Hönel D, et al. New recording materials for the holographic industry. Proc SPIE 2009;7233:72330K–72330K–10. doi:10.1117/12.809579.

[11] Marín-Sáez J, Atencia J, Chemisana D, Collados M-V. Characterization of volume holographic optical elements recorded in Bayfol HX photopolymer for solar photovoltaic applications. Opt Express 2016;24:A720. doi:10.1364/OE.24.00A720.

[12] Bruder F-K, Fäcke T, Grote F, Hagen R, Hönel D, Koch E, et al. Performance optimization in mass production of volume holographic optical elements (vHOEs) using Bayfol HX photopolymer film. In: Hrabovský M, Sheridan JT, Fimia A, editors. Proc. SPIE, 2017, p. 102330G. doi:10.1117/12.2265022.

[13] Cody D, Gul S, Mikulchyk T, Irfan M, Kharchenko A, Goldyn K, et al. Self-processing photopolymer materials for versatile design and fabrication of holographic sensors and interactive holograms. Appl Opt 2018;57:E173. doi:10.1364/AO.57.00E173.

[14] Liu H, Yu D, Zhou K, Wang S, Luo S, Wang W, et al. Improvement of temperature-induced spectrum characterization in a holographic sensor based on N-isopropylacrylamide photopolymer hydrogel. Appl Opt 2017;56:9006. doi:10.1364/AO.56.009006.

[15] Tomita Y, Nakamura T, Tago A. Improved thermal stability of volume holograms recorded in nanoparticle–polymer composite films. Opt Lett 2008;33:1750. doi:10.1364/OL.33.001750.

[16] Russo JM, Kostuk RK. Temperature dependence properties of holographic gratings in phenanthrenquinone doped poly(methyl methacrylate) photopolymers. Appl Opt 2007;46:7494. doi:10.1364/AO.46.007494.

[17] Dhar L, Schnoes MG, Wysocki TL, Bair H, Schilling M, Boyd C. Temperature-induced changes in photopolymer volume holograms. Appl Phys Lett 1998;73:1337–9. doi:10.1063/1.122375.

[18] Zanutta A, Bianco A, Insausti M, Garzón F. Volume phase holographic gratings for astronomy based on solid photopolymers. In: Navarro R, Cunningham CR, Barto AA, editors. Proc. SPIE, 2014, p. 91515X. doi:10.1117/12.2055743.

[19] Felder TC, Stevenson SH, O'Connor PJ, Yohannan, Jr. RM. Environmental Performance of Photopolymer Holographic Optical Elements. In: Benton SA, Stevenson SH, Trout TJ, editors. Proc. SPIE, 2000, p. 314–23. doi:10.1117/12.380011.

[20] Chrysler BD, Ayala Pelaez S, Wu Y, Vorndran SD, Kostuk RK. Environmental stability study of holographic solar spectrum splitting materials. In: Sulima O V., Conibeer G, editors. Proc. SPIE, 2016, p. 99370N. doi:10.1117/12.2237071.

[21] Syms R. Practical Volume Holography. Oxford University Press; 1990.

[22] Marín-Sáez J, Collados MV, Atencia J, Chemisana D. Optical and Energetic Performance of Volume Holographic Optical Elements for Solar Energy Applications. Adv. Energy Res., NOVA; 2017.

[23] Bañares-Palacios P, Álvarez-Álvarez S, Marín-Sáez J, Collados M-V, Chemisana D, Atencia J. Broadband behavior of transmission volume holographic optical elements for solar concentration. Opt Express 2015;23:A671–81. doi:10.1364/OE.23.00A671.

[24] Sallaberry F, Pujol R, Garcia de Jalón A. Direct Tracking Error Estimation on a 1-Axis Solar Tracker. Proc. EuroSun 2014 Conf., Freiburg, Germany: International Solar Energy Society; 2015, p. 1–8. doi:10.18086/eurosun.2014.16.20.

[25] Covestro Deutschland AG. Bayfol HX200 Datasheet. 2016.

[26] MaterialScience B. Bayfol HX102 Datasheet. 2014.